



Textural and electronic structure engineering of carbon nitride via doping with π -deficient aromatic pyridine ring for improving photocatalytic activity



Zhihong Chen, Peng Sun, Bing Fan, Qiong Liu, Zhengguo Zhang, Xiaoming Fang*

Key Laboratory of Enhanced Heat Transfer and Energy Conservation, The Ministry of Education, School of Chemistry and Chemical Engineering, South China University of Technology, Guangzhou 510640, China

ARTICLE INFO

Article history:

Received 2 December 2014

Received in revised form 15 January 2015

Accepted 19 January 2015

Available online 20 January 2015

Keywords:

Carbon nitride

Molecule doping

π -Deficient pyridine ring

DFT calculations

Photocatalytic activity

ABSTRACT

Molecular doping of conjugated carbon nitride (CN) with π -deficient pyridine ring was applied for the modification of CN photocatalysts. According to the density functional theory (DFT) calculations, the incorporation of π -deficient pyridine ring entities in the conjugated CN matrix can effectively modulate the intrinsic electronic and band structure of CN by relocating its π -electrons. And then, a series of pyridine-doped CN photocatalysts were synthesized via thermal copolymerizing dicyandiamide (DCDA) with 2, 6-diaminopyridine (DPY). Integrating π -deficient pyridine ring into the CN network by modification with DPY does not alter the crystal structures or the core chemical skeleton of CN. A significant alteration in the texture and morphology was also observed for the modified CN samples. Moreover, integrating π -deficient pyridine ring into the conjugated CN network can actually engineer the electronic structure with tunable band-gap and promotes the migration and separation of photo-generating electron-hole pairs, which are in well agreement with the theoretical calculation results. The combined benefits of the molecular doping in terms of electronic, optical, surface and texture properties lead to a significant improvement in the photocatalytic activity for methyl orange (MO) degradation under visible light irradiation. The $O_2^{\bullet-}/^{\bullet}OOH$ radical is the major oxidation species in the photocatalytic oxidation process. The modulated CN incorporating π -deficient aromatic systems possess a higher reduction potential because the extension of optical absorption of CN mostly results from the up-shift of HOMO, which is favorable for the photocatalytic degradation of organic pollutant.

© 2015 Elsevier B.V. All rights reserved.

1. Introduction

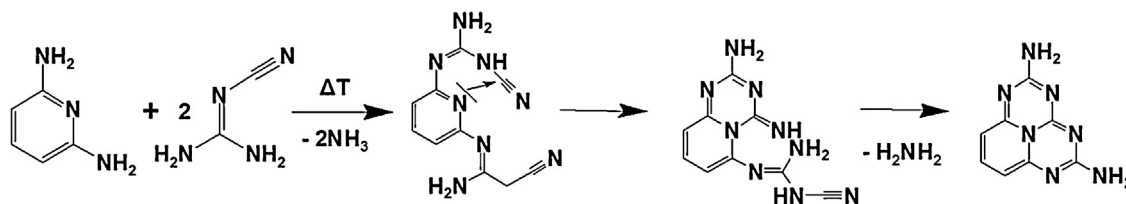
Semiconductor-based photocatalysis has been considered to be an ideal way for photocatalytic H_2 production from water splitting [1] and degradation of pollutants [2], owing to its advantages of low-cost and environmentally friendly. However, low quantum yield and solar energy utilization efficiency are the main constraints on the practical applications of photocatalysis. Therefore, high-efficiency semiconductor photocatalysts need to be developed, especially the visible-light-driven ones.

Recently, a lot of attention has been paid to a visible-light-driven metal-free polymeric photocatalyst, graphitic carbon nitride (g-CN), which has been shown to function as a semiconductor with an intrinsic band gap of 2.7 eV, having suitable band positions covering water splitting potentials [3,4]. However, being an organic

aromatic π -conjugated semiconductor, the carbon nitride photocatalyst is greatly limited by its relatively fast charge recombination and insufficient absorption of sunlight.

Various strategies, such as microstructure regulations [5–10], heterojunction [11–17], doping [18–22], and copolymerization [23–30] have been exploited to improve the photocatalytic activity and adjust selectivity photocatalytic activity of CN. Among those strategies, copolymerization that another organic monomer is mixed with the precursor during the preparation of CN has been regarded as an efficient route, not only for modulating the electronic and band structure of CN via control its π -conjugated aromatic system, but also for creating surface dyadic heterostructures to promote splitting and separation of the separated electrons and holes at the materials surface, thus leading to an enhancement in its photocatalytic activity. More importantly, this copolymerization method can be readily guided by theoretical calculations, a versatile tool to understand and manipulate carbon nitride substructures. Up to now, lots of organic monomers with specific structures, such as 2-aminobenzonitrile [23], tetraphenylboron

* Corresponding author. Tel.: +86 20 87112997; fax: +86 20 87113870.
E-mail address: cexmfang@scut.edu.cn (X. Fang).



Scheme 1. Processes of copolymerization reactions between dicyandiamide and DPY.

[26], barbituric acid [28], and thiophene [29,30], have been used for integrating difference functional aromatic ring into the CN frameworks. However, those previous studies have been almost focused on incorporating the CN frameworks with conjugated functional groups with π -conjugated aromatic systems [23], such as benzene and its derivatives, and those with π -rich aromatic systems [29,30], such as thiophene and its derivatives. Little attention has been paid on integrating the CN frameworks with conjugated functional groups with π -deficient aromatic systems. Since the π -deficient aromatic ring whose π -electron cloud intensity is lower than that of benzene is an important part in the aromatic system, it is of significance to carry out a systematic research on the modification mechanism and the influence of incorporating conjugated functional groups with π -deficient aromatic systems into CN frameworks for improving photocatalytic activity.

Pyridine ring is a typical π -deficient aromatic functional group, which π -electrons are delocalized over the ring because of the negative inductive effect of the nitrogen atom. In the current work, pyridine-doped CN photocatalysts were successfully synthesized by copolymerizing dicyandiamide (DCDA) with a pyridine derivative, 2,6-diaminopyridine (DPY). According to density-functional-theory (DFT) calculations, the highest occupied molecular orbital (HOMO) and the lowest unoccupied molecular orbital (LUMO) of CN can be precisely chemically engineered through incorporating pyridine into CN frameworks, so that the resulting bandgap will be narrowed to improve photonic efficiency. The influence of pyridine on the morphologies, structures, optical absorption properties, emission features and photoelectrochemical behaviors of pyridine-doped CN were carefully investigated. And the photocatalytic activities of the pyridine-doped CN photocatalysts have been evaluated. It is found that the photocatalytic activities of the doped CN samples are superior to that of CN. This work may provide a common and simple route along with an insight into modulating the structure and properties of CN via incorporation conjugated functional groups with π -deficient aromatic systems into CN frameworks for improving its photocatalytic activity.

2. Experimental

2.1. Preparation of CN and doped CN

CN was prepared by calcining dicyandiamide (Alfa Aesar) at 550 °C for 4 h at a heating-rate of 15 °C/min via the thermal polymerization process [23].

The route for the copolymerization reaction between dicyandiamide and DPY (Alfa Aesar) is displayed in Scheme 1. The carbon atoms of the co-monomer DPY undergo the nucleophilic attack on the amino groups of dicyandiamide to form a similar structure to that of melem, which is known to be an important intermediate of the polymer CN. Simultaneously, the polymerization between two molecules of dicyandiamide takes place to form melem. As a result, the DPY-doped CN was obtained. In a typical synthesis, dicyandiamide (3 g) was mixed with different amounts of DPY dispersed in 15 mL water, followed by heating to 100 °C under stirring

to remove water. The obtained solids were calcined at 550 °C for 4 h at a heating-rate of 15 °C/min to obtain a series of DPY-doped CN samples denoted as CN-DPY_w, where *w* represents the mass fractions of DPY in the samples and has been set at 0.01, 0.03, 0.05, 0.07, and 0.10.

2.2. Characterizations

Powder X-ray diffraction (XRD) data were obtained from a D/max-III A X-ray diffractometer. Fourier transform infrared spectroscopy (FT-IR) was recorded on a Vector 33 infrared Fourier spectrometer. The solid-state ¹³C NMR spectra were recorded using a Bruker Advance III 500 spectrometer. Electron paramagnetic resonance (EPR) measurements were recorded using a Bruker model A300 spectrometer with a 300 W Xe lamp equipped with an IR-cutoff filter (<800 nm) and a UV-cutoff (>420 nm) as visible light source. The Brunauer–Emmett–Teller (BET) surface area was measured on a Micromeritics ASAP 2020. Transmission electron microscopy (TEM) images were obtained by using a JEM2100F field emission electron microscope. The diffuse reflection spectra (DRS) were obtained from a U-3010 spectrophotometer. PL spectra of the photocatalyst powers were measured at room temperature using an F-4500 Fluorescence Spectrophotometer equipped with solid sample holder and the excitation wavelength is 325 nm.

2.3. Photocatalytic activity

The photocatalytic degradation of methyl orange under visible light was applied to evaluate the photocatalytic activity of the doped CN photocatalysts. 0.1 g of each sample was added into 100 mL of methyl orange aqueous solution with a concentration of 10 mg/L. The suspensions were stirred for 30 min in the dark to reach saturated adsorption of methyl orange. Then visible irradiation provided by a 300 W Xe lamp (output light intensity is 1 sun, AM 1.5, 100 mW cm⁻²) with a 420 nm cut-off filter was introduced to the suspensions. At time intervals of each one hour, samples were taken and centrifuged to remove the catalysts. The concentrations of methyl orange were then detected using a UV-2450 spectrophotometer. In order to detecting the active species during the photocatalytic reaction, isopropanol (IPA), and benzoquinone (BQ) were added into the MO solution dispersed with the CN-DPY system to capture hydroxyl radicals ($\cdot\text{OH}$) and the superoxide radicals ($\text{O}_2^{\cdot-}$), respectively, followed by the photocatalytic activity test. Moreover, N₂ and O₂ were bubbling in the photocatalytic reaction systems, respectively, followed by the photocatalytic activity test. Signals of radicals spin trapped by 2,2,6,6-tetramethylpiperidinyloxy (TEMPO) were obtained using a Bruker model ESP 300 E electron paramagnetic resonance spectrometer equipped with a xenon lamp (with 420 nm filter) as the light source.

2.4. Electrochemical analysis

Film electrodes used in electrochemical measurements were fabricated by the doctor-blading method as follows. The as-prepared catalysts were grinded into fine slurries in an ethyl

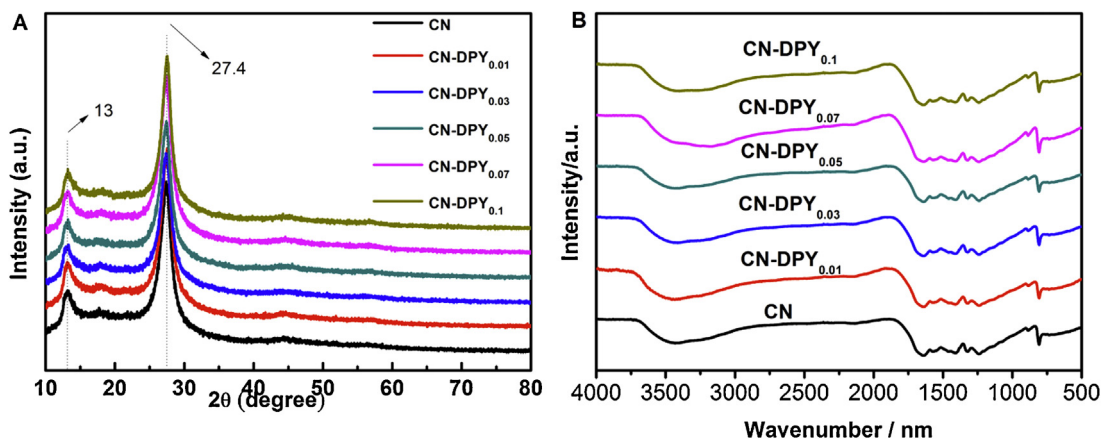


Fig. 1. XRD (A) patterns and FT-IR spectra (B) of pure CN and DPY-doped CN samples with different mass fractions of DPY.

cellulose ethanol solution, and then the slurries were doctor-bladed onto fluoride-tin oxide (FTO) conductive glass sheet, respectively. After being dried in the air, the film electrodes of the undoped and DPY-doped CN photocatalysts were obtained. The electrochemical properties were performed in a conventional three-electrode cell using an electrochemical analyzer (CS-350, Wuhan CorrTest, China). The working electrode was immersed in a sodium sulfate electrolyte solution (0.1 M), using a Pt sheet and an Ag/AgCl electrode as the counter and reference electrodes, respectively. 1 M NaSO₄ aqueous solution was used as the supporting electrolyte. The working electrode was irradiated from the back side (FTO substrate/semiconductor interface) to minimize the influence of the thickness of the semiconductor layer. The exposed area under illumination was 0.2 cm². The periodic on/off photocurrent response of CN-DPY_{0.07} and CN modified fluorine-doped tin oxide glass (FTO) at 0.4 V bias vs. Ag/AgCl, the perturbation signal was 10 mV with the frequency at 1 kHz. For electrochemical impedance spectroscopy (EIS) experiments, the perturbation signal was also 10 mV, but the frequency ranged from 200 kHz to 10 mHz.

2.5. DFT calculations

In order to elucidate the electronic distribution and band structure of DPY-doped CN, DFT calculations have been carried out using Gaussian09 program, employing the B3LYP functionals and 6–31G (d, p) basis set for all the atoms in the DFT calculations [31]. The smallest unit with a pore (trimers of CN and CN-DPY) has been selected as the calculation model to simulate the band structures (HOMO and LUMO) of CN and DPY-doped CN. The structural optimizations have been performed without any symmetry constraints.

3. Results and discussion

3.1. Structure and morphology of DPY-doped CN

Fig. 1 shows the XRD patterns and FT-IR spectra of the pyridine-doped CN samples at different mass fractions of DPY, together with those of CN. Two distinct diffraction peaks are found in all the samples, which can be ascribed to the typical diffraction peaks of CN (JCPDS 87-1526). The stronger peak at 27.1° can be indexed as the (002) diffraction peak and represents the inter-planar graphitic stacking with an inter-layer distance of 0.33 nm. The minor peak at around 13.1° corresponds to the (100) diffraction peak and represents an inter-planar separation of 0.68 nm. Further, similar FT-IR spectra related to the CN heterocycles skeletal vibration are observed for CN and CN-DPY. The typical breathing and stretching vibration modes of the heptazine heterocyclic ring (C₆N₇) are

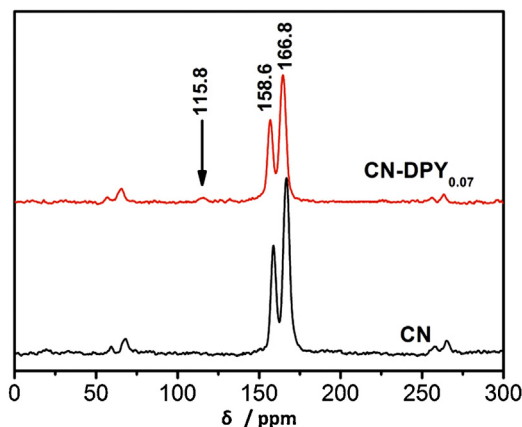


Fig. 2. Solid-state ¹³C NMR spectra for CN and CN-DPY_{0.07} samples.

located at 810 cm⁻¹ and 1200–1600 cm⁻¹, respectively, confirming the formation of a triazine phase in all samples. The broad band at 2900–3500 cm⁻¹ is ascribed to the adsorbed O–H molecules and N–H vibration due to the surface uncondensed amine groups. The similar XRD distinct diffraction peaks and FT-IR vibration modes of DPY-doped CN to those of pure CN indicate that, the copolymerization of DPY with dicyandiamide does not alter the structural integrity of CN, such as the core crystal structure and core chemical skeleton integrity, which are necessary for exhibiting high photocatalytic activity.

The C/N molar ratios of pure CN and DPY-doped CN samples have been obtained from XPS and are listed in Table 1. A gradual increase in the C/N molar ratio from 0.73 for pristine CN to 0.76 for CN-DPY_{0.07} reveals the successful integration of the π -deficient aromatic pyridine ring in the CN-conjugated network. These additional carbon species were further characterized by solid-state ¹³C NMR spectra, as shown in Fig. 2. A new broad peak centered at 115.8 ppm is clearly observed for the CN-DPY sample, suggesting the incorporation of aromatic pyridine carbon species in the CN-conjugated network. As another result of the pyridine doping, the signal ratio of between the chemical shifts of 158.6 and 166.8 ppm in the ¹³C NMR spectra increases from 0.5 for CN to 0.57 for DPY-doped CN.

The BET surface area of the pure and doped CN samples has been measured and is listed in Table 1. The surface area of DPY-doped CN is larger than that of pristine CN and increases gradually with the DPY content, suggesting that the DPY monomers play a very important role in the process of carbon nitride polymerization. Fig. 3A shows the N₂-sorption isotherms of CN and CN-DPY_{0.07}. As shown in Table 1, the surface area increases rapidly when the amount of

Table 1

Physicochemical properties and apparent rate constant of the as-prepared samples for degrading MO.

Sample	C/N mole ratio	Surface area ^a (m ² /g)	Band-gap ^b eV	Rate constant 10 ⁻² k (h ⁻¹)
CN	0.73	13.167	2.81	8.70
CN-DPY _{0.01}	0.73	14.604	2.72	10.01
CN-DPY _{0.03}	0.73	15.742	2.67	13.69
CN-DPY _{0.05}	0.74	17.733	2.40	14.77
CN-DPY _{0.07}	0.75	19.542	2.26	18.79
CN-DPY _{0.10}	0.76	32.899	2.19	12.12

^a Calculated from N₂ absorption–desorption isotherms.^b Estimated from optical measurements.

DPY adds up to 0.1 g, because the excess DPY, which did not undergo the nucleophilic attack on the amino groups of dicyandiamide, would decompose and release much gas, such as CO₂ and NH₃ in the process of carbon nitride polymerization. Moreover, TEM has been employed to observe the microstructure of the DPY-doped CN. Fig. 3 displays the typical TEM images of CN (A) and CN-DPY_{0.07} (B). As seen from TEM images of the as prepared-samples, the surface morphology is greatly changed with integrating pyridine donors in the CN skeleton. After the copolymerization with DPY, the compact stacking of tri-s-triazine-based layered sheets for CN becomes much looser and more poriferous, resulting in the enlarged surface area of DPY-doped CN.

3.2. Optical properties and band structure of DPY-doped CN

The optical absorption and emission features of the pure CN and DYP-doped CN samples have been monitored by the diffuse reflection and photoluminescence spectra experimentally, as shown in Fig. 4. The photographs of the samples are inserted in Fig. 4. The optical absorption exhibits a remarkable shift to longer wavelength with increasing in the mass fractions of DPY. Specifically, the absorption edge is shifted from 460 nm for CN to 700 nm for CN-DPY_{0.10}, corresponding to the change of sample color from yellow to brown, indicating that the DYP-doped CN samples really exhibit better visible-light absorption properties. In addition, the peak position and photoluminescence intensity of CN and CN-DPY samples are also greatly changed by the molecular doping, as shown in Fig. 4B. The emission peak of CN-DPY solids gradually shifts toward longer wavelength (from 482 nm to 565 nm) with continuing increasing DPY content, implying a reduction in the HOMO–LUMO gap for DPY-doped CN. Simultaneously, obvious fluorescence quenching is also observed for pyridine-doped samples, suggesting that the extended π -conjugation system with a CN-heterostructure at material interfaces can effectively reduce the

recombination of photo-generating electron–hole pairs. A residual signal at 482 nm is observed for the DPY-doped CN, due to the insufficient amount of DPY monomer to copolymerize with DCDA. Moreover, the PL intensity increase as the DPY content increase to 0.1 g, which would be attributed to excessive amount of co-monomer lead to more lattice defect to be the center of charge carrier recombination.

DFT calculations were carried out to elucidate the electronic distribution and band structure of CN and DYP-doped CN. Fig. 5 illustrates the electronic structure of polymeric trimer models including the optimized HOMO and LUMO for CN trimer (a) and DPY-doped CN trimer (b), and their corresponding DFT calculated HOMO–LUMO gap (c). It is well known that the HOMO and LUMO in a cluster are the counterparts of VB and CB levels in the material. For the pristine trimer, HOMO is chiefly derived from the combination of nitrogen p_z orbitals, while LUMO predominantly localizes in C–N bond orbitals (Fig. 5a) [3,23]. From Fig. 5b, it can be clearly found that the HOMO of CN shifts to locate between the tri-s-triazine subunit and the copolymerized pyridine segment after incorporating π -deficient pyridine ring into the CN frameworks, whereas LUMO still retains in C–N bond orbitals. Consequently, grafting pyridine hetero-molecules on CN framework can effectively relocate the π -electrons to modulate the corresponding HOMO, while the corresponding LUMO just change a little. The reconstruction of π -conjugated electrons induces the slight down-shift of LUMO with 0.068 eV and simultaneously the strong up-shift of HOMO with 0.288 eV, reducing the bandgap energy by 0.356 eV altogether. The reducing bandgap is largely ascribed to the evident up-shift of HOMO after integrating pyridine into the CN framework, which is very favorable for retaining the high reduction potential of pyridine-doped CN. Furthermore, HOMO and LUMO turn to be non-coplanar when the π -deficient pyridine groups have been integrated into CN, facilitating the charge separation of photogenerated carriers and thus benefiting the photocatalytic performance.

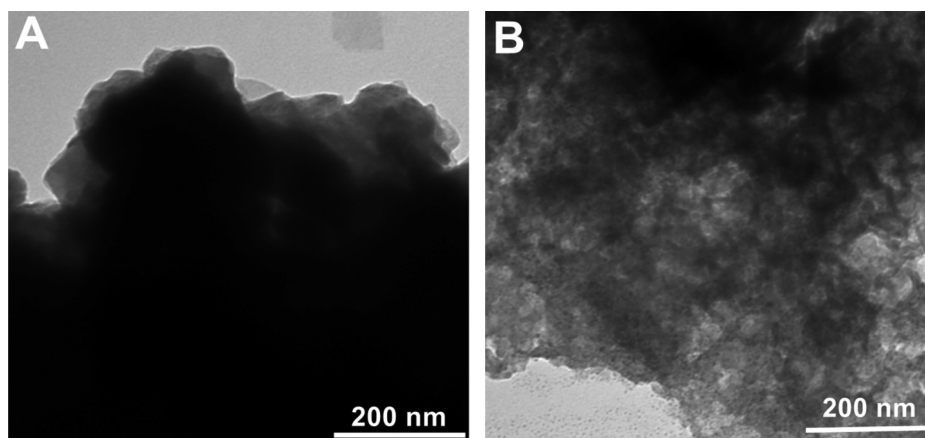


Fig. 3. Typical TEM images of CN (A) and CN-DPY_{0.07} (B) and their corresponding N₂-sorption isotherms (C).

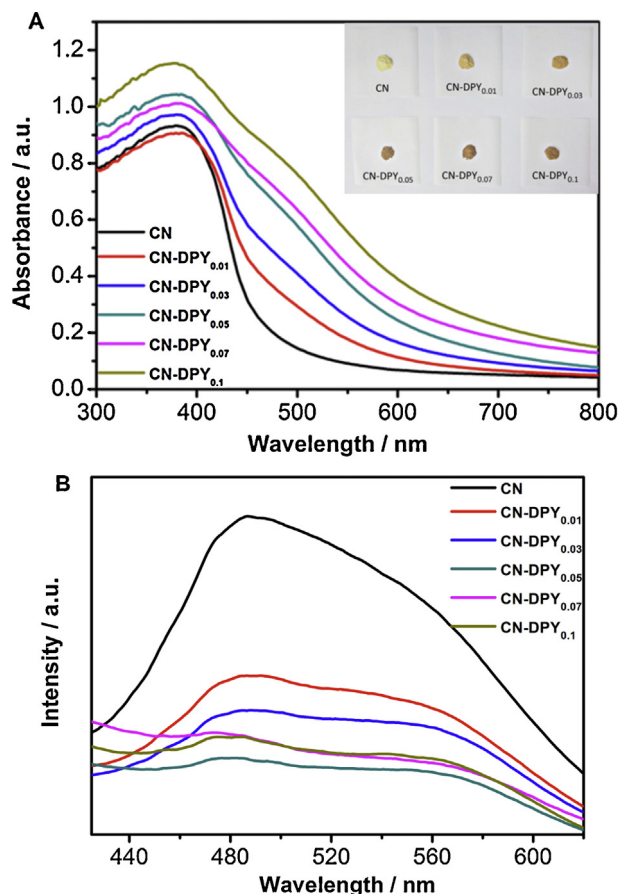


Fig. 4. Diffuse reflection (A) and photoluminescence (B) spectra of pure CN and DPY-doped CN samples with different mass fractions of DPY; inset is the photograph of the as-prepared samples.

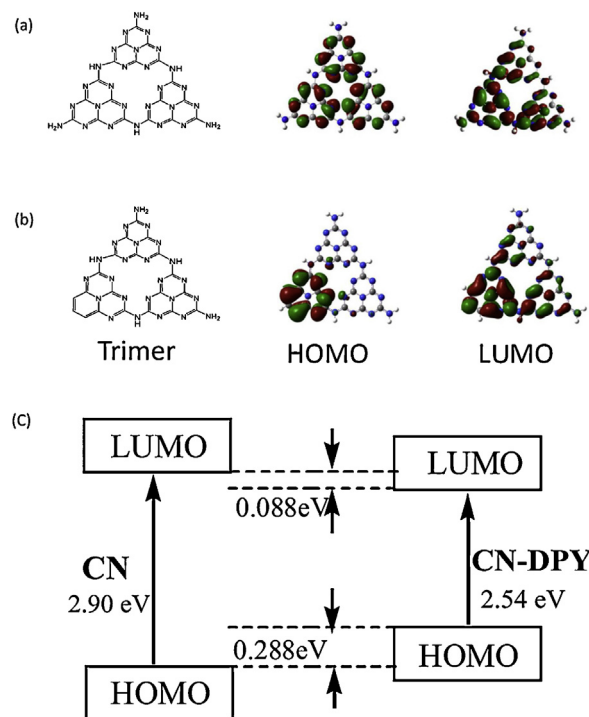


Fig. 5. Electronic structure of polymeric trimer models including the optimized HOMO and LUMO for CN trimer (a) and DPY-doped CN trimer (b), and their corresponding DFT calculated HOMO–LUMO gap (c).

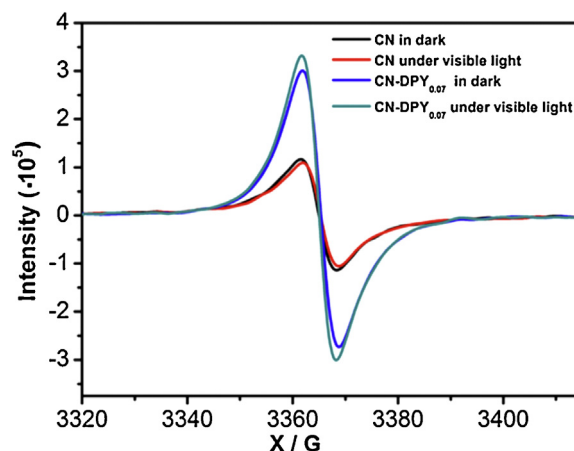


Fig. 6. EPR spectra of CN and CN-DPY_{0.07} samples in the dark and under visible light irradiation (>420 nm).

Moreover, the evolution of the electronic band structure for pyridine-doped CN has been further verified by electron paramagnetic resonance (EPR) spectra experimentally, as shown in Fig. 6. Only one single Lorentzian line centered at a g value of 2.0034 both in dark and visible light irradiation are observed for the CN and CN-DPY_{0.07} samples [32], demonstrating a well-established CN semiconductor structure even for the pyridine-doped samples. These Lorentzian lines originate from the unpaired electron on the carbon atoms of the aromatic rings within π -bonded nanosized clusters. The EPR signal intensity of CN-DPY_{0.07} is 298421, about 3 times that of CN (109770). Obviously, the EPR intensities of CN-DPY_{0.07} are extremely amplified, elucidating the effective extension of delocalized systems of CN heterocycles after integrating pyridine ring into the CN framework via modified with DPY, as already illustrated by DFT calculations. Both enhanced EPR signal were observed when CN and CN-DPY_{0.07} were irradiated with visible light, indicating the efficient photochemical generation of radical pairs in the semiconductor. And the EPR signal intensity of CN-DPY_{0.07} increase about 13% (from 298421 to 337154), much higher than that of CN (about 5%, from 109770 to 115400), indicating that the CN-DPY_{0.07} can be excited to generated electron–hole pairs more easily under visible light irradiation. This is a convincing symptom to predict the efficient generation of photochemistry radical pairs occurred in pyridine-doped CN, being beneficial for heterogeneous photocatalytic reactions.

3.3. Photocatalytic activity and stability of DPY-doped CN

Fig. 7 and Table 1 show the photocatalytic degradation curves of MO in presence of the doped CN samples under visible light irradiation, together with that in presence of CN for comparison purposes. Under visible light irradiation, all the pyridine-doped CN showed higher photocatalytic activity than that of the pristine CN, which can be attributed to the higher surface area, wider optical absorbance and improving photo-generating electron–hole separation. Moreover, the charge generation and separation properties of the as prepared samples were examined by photo-electrochemical experiments to investigate the factors influencing photocatalytic activity, as shown in Fig. 8. The photocurrent intensity of the CN is improved after doping with DPY, indicating the efficient photogenerated charge generation of the pyridine-doped samples. Significant decrease in semicircular Nyquist plots is observed for pyridine-doped samples in the dark, clearly demonstrating that incorporating aromatic pyridine in CN skeleton indeed can effectively improve the electronic conductivity of polymer matrix to promote the charge separation. Interestingly, the surface area and

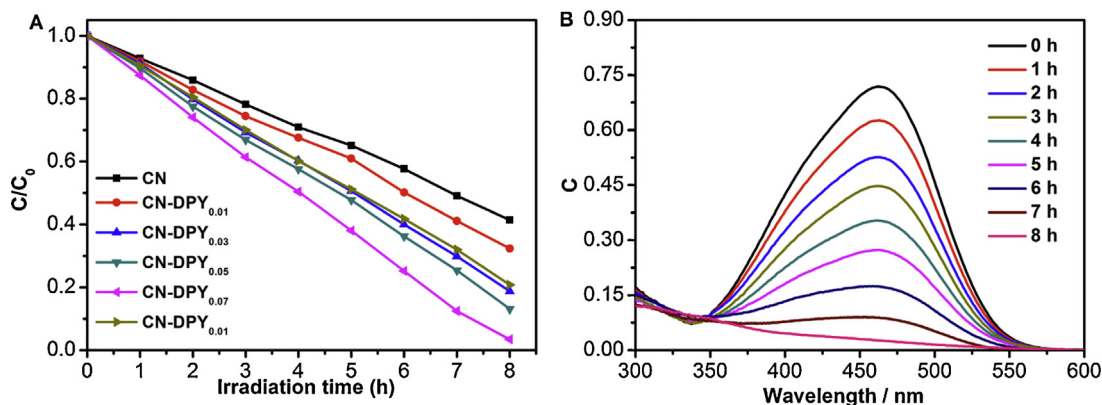


Fig. 7. Photocatalytic activities of pure CN and pyridine-doped CN samples with different mass fractions of DPY (A) and typical temporal absorbance spectrum changes of MO in the presence of CN-DPY_{0.07} (B) under visible light irradiation.

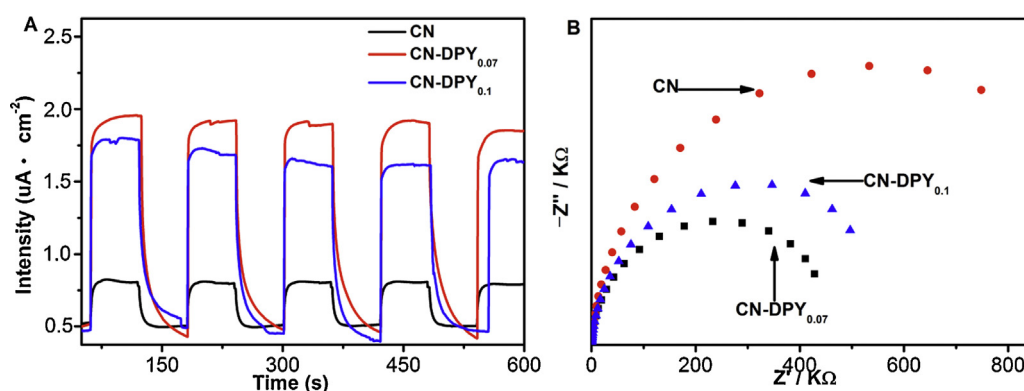


Fig. 8. Periodic on/off photocurrent response under visible light irradiation (A) and electrochemical impedance spectroscopy plots in the dark (B).

optical absorbance will improve significantly but the photocatalytic activity decrease rapidly when the DPY content further increase to 0.1 g. This is because fast charge recombination of CN-DPY_{0.1} will offset the effect of high surface area and wide optical absorbance, which well is verified by the PL and EIS experiments results. Based on the above results, it can be clearly found that higher surface area, wider optical absorbance and faster charge separation work together to improve the photocatalytic activity of CN after integrated pyridine into CN framework, and the enhanced charge separation is the main influent factor.

To evaluate the stability and reusability of the CN-DPY photocatalyst, we carried out the additional experiments to degrade MO under visible light cycled for five times (Fig 9). A slight deactivation was noticed in the first five runs, which indicates that CN-DPY has high stability in the photocatalytic oxidation (PCO) process under visible light irradiation.

3.4. Photocatalytic mechanism of DPY-doped CN

In the PCO process, a series of reactive oxygen species, such as $\cdot\text{OH}$, $\text{O}_2^{\cdot-}/\cdot\text{OOH}$, or H_2O_2 are supposed to be involved. To distinguish the reactive oxy-radical, photocatalytic experiments were performed under different atmospheres [33,34], as shown in Fig. 10A. Isopropanol (IPA) and benzoquinone (BQ) acted as the efficient scavengers for $\cdot\text{OH}$, $\text{O}_2^{\cdot-}/\cdot\text{OOH}$ were introduced into the PCO process, respectively. Addition of IPA in the MO solution has little effect on the photocatalytic activity of CN-DPY_{0.07}, suggesting that $\cdot\text{OH}$ does not play a key role for the degradation of MO. On the contrary, the photocatalytic degradation of MO is completely inhibited after the addition of BQ. It was observed that the degradation rate

of MO was depressed under an N_2 atmosphere but improved when conducted in the presence of bubbling O_2 , suggesting that the dissolved O_2 in the solution acted as electron trapper, leading to the generation of active oxygen species $\text{O}_2^{\cdot-}/\cdot\text{OOH}$. Based on those results, it can be concluded that $\text{O}_2^{\cdot-}/\cdot\text{OOH}$ are the main oxygen active species for CN-DPY_{0.07} in the MO solution under visible light irradiation. Moreover, the singlet oxygen radical ($^1\text{O}_2$) was investigated by an ESR spin-trap technique (with TEMPO) in the reaction system under visible light irradiation (Fig 10B). The intensity of TEMPO \cdot signals increased under visible light irradiation,

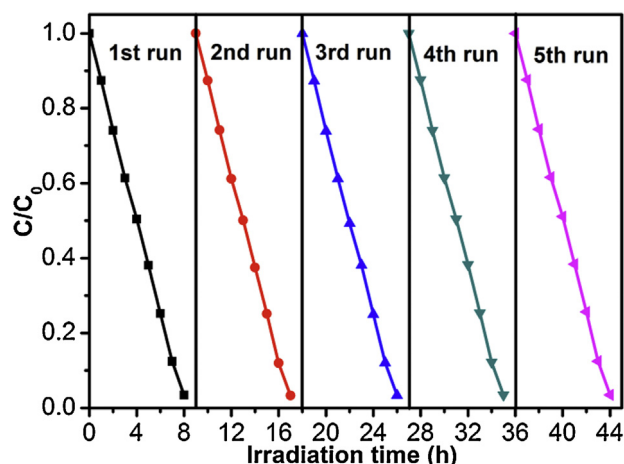


Fig. 9. Cycle runs of CN-DPY_{0.07} for MO degradation under visible light irradiation.

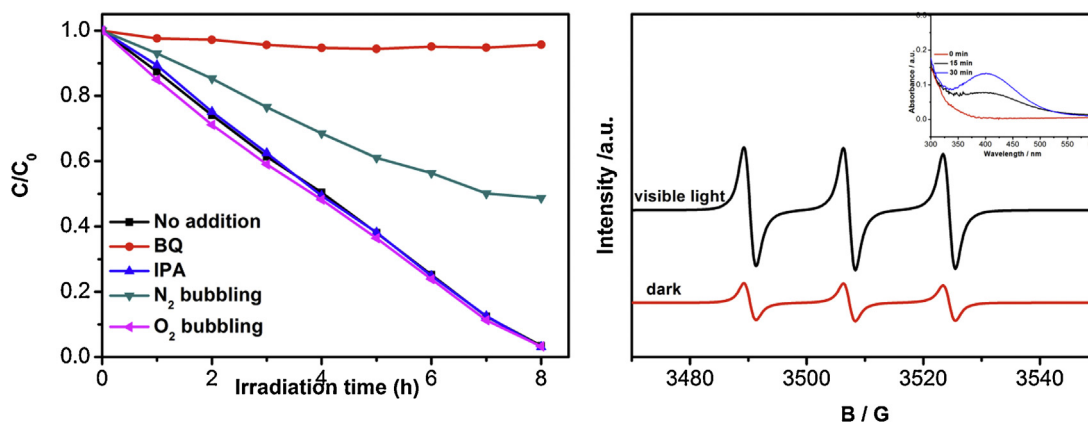


Fig. 10. Photocatalytic activities of CN-DPY_{0.07} on the degradation of MO in presence of different scavengers under visible light irradiation (A) and TEMPO- 1O_2 adducts (B) of CN-DPY_{0.07} in the dark or under visible light, inset is the absorption spectrum of $Ti(IV)-H_2O_2$ generated by CN-DPY_{0.07} in H_2SO_4 solution (pH 1) under visible light.

supporting the generation of singlet oxygen with the superoxide radical ($2O_2^{\bullet-} + 2H^+ \rightarrow ^1O_2 + H_2O_2$). The production of H_2O_2 was checked by a colorimetric titration method using the formation of the yellow colored $Ti(IV)-H_2O_2$ complex under acidic reaction conditions. The characteristic absorption peak at $\lambda = 410$ nm was found, supporting the production of H_2O_2 . According to the above results, it can clearly draw the conclusion that $O_2^{\bullet-}/^{\bullet}OOH$ is the major oxidation species in the photocatalytic oxidation process.

4. Conclusion

In summary, pyridine-doped CN photocatalysts have been successfully synthesized by copolymerizing dicyandiamide with 2,6-diaminopyridine and systematically investigated by theoretical calculations and experiment. Both textural structure and electronic structure of CN photocatalyst can be greatly controlled via molecular doping of its conjugated frameworks with π -deficient pyridine rings. Integrating π -deficient pyridine ring into the CN network by modification with DPY does not alter the crystal structures or the core chemical skeleton of CN but the texture and morphology. The incorporation of pyridine in CN skeleton can effectively extend and delocalize the aromatic π -conjugated system, adjusting its intrinsic semiconductor properties, such as engineering the band structure with tunable bandgap and facilitating the migration and separation of photo-generating electron-hole pairs. Hence, as a result of pyridine doping, an overall enhanced photocatalytic activity is achieved. The $O_2^{\bullet-}/^{\bullet}OOH$ radical is the major oxidation species in the photocatalytic oxidation process. The modulated CN incorporating π -deficient aromatic systems possess a higher reduction potential because the extension of optical absorption of CN mostly results from the up-shift of HOMO, which is favorable for the photocatalytic degradation of organic pollutant. This work may provide a common and simple route along with an insight into modulating the structure and properties of CN via incorporation conjugated functional groups with π -deficient aromatic systems into CN frameworks for improving its photocatalytic activity.

Acknowledgements

This work is supported by the National Natural Science Foundation of China (Project Number 60976053 and 21276088). Thanks are due to Yingying Yao from Institute of Process Engineering, Chinese Academy of Science, for her help in DFT calculations.

References

- [1] X.B. Chen, S.H. Shen, L.J. Guo, S.S. Mao, Chem. Rev. 110 (2010) 6503–6570.
- [2] H. Tong, S.X. Ouyang, Y.P. Bi, N. Umezawa, M. Oshikiri, J.H. Ye, Adv. Mater. 24 (2012) 229–251.
- [3] X.C. Wang, K. Maeda, A. Thomas, K. Takanabe, G. Xin, J.M. Carlsson, K. Domen, M. Antonietti, Nat. Mater. 8 (2009) 76–80.
- [4] Y. Wang, X. Wang, M. Antonietti, Angew. Chem. Int. Ed. 51 (2012) 68–89.
- [5] A. Thomas, A. Fischer, F. Goettmann, M. Antonietti, J.O. Muller, R. Schlögl, J.M. Carlsson, J. Mater. Chem. 18 (2008) 4893–4908.
- [6] X.C. Wang, K. Maeda, X.F. Chen, K. Takanabe, K. Domen, Y.D. Hou, X.Z. Fu, M. Antonietti, J. Am. Chem. Soc. 131 (2009) 1680.
- [7] X.H. Li, J.S. Zhang, X.F. Chen, A. Fischer, A. Thomas, M. Antonietti, X.C. Wang, Chem. Mater. 23 (2011) 4344–4348.
- [8] X.H. Li, X.C. Wang, M. Antonietti, Chem. Sci. 3 (2012) 2170–2174.
- [9] P. Niu, L.L. Zhang, G. Liu, H.M. Cheng, Adv. Funct. Mater. 22 (2012) 4763–4770.
- [10] X.J. Bai, L. Wang, R.L. Zong, Y.F. Zhu, J. Phys. Chem. C 117 (2013) 9952–9961.
- [11] L. Ge, C.C. Han, J. Liu, Appl. Catal. B 108 (2011) 100–107.
- [12] L. Ge, C.C. Han, J. Liu, J. Mater. Chem. 22 (2012) 11843–11850.
- [13] H.W. Kang, S.N. Lim, D. Song, S.B. Park, Int. J. Hydrogen Energy 37 (2012) 11602–11610.
- [14] C.S. Pan, J. Xu, Y.J. Wang, D. Li, Y.F. Zhu, Adv. Funct. Mater. 22 (2012) 1518–1524.
- [15] L.M. Sun, X. Zhao, C.J. Jia, Y.X. Zhou, X.F. Cheng, P. Li, L. Liu, W.L. Fan, J. Mater. Chem. 22 (2012) 23428–23438.
- [16] S.W. Cao, Y.P. Yuan, J. Fang, M.M. Shahjamali, F.Y.C. Boey, J. Barber, S.C.J. Loo, C. Xue, Int. J. Hydrogen Energy 38 (2013) 1258–1266.
- [17] Z.H. Chen, P. Sun, B. Fan, Z.G. Zhang, X.M. Fang, J. Phys. Chem. C 118 (2014) 7801–7807.
- [18] X.C. Wang, X.F. Chen, A. Thomas, X.Z. Fu, M. Antonietti, Adv. Mater. 21 (2009) 1609.
- [19] G. Liu, P. Niu, C.H. Sun, S.C. Smith, Z.G. Chen, G.Q. Lu, H.M. Cheng, J. Am. Chem. Soc. 132 (2010) 11642–11648.
- [20] S.C. Yan, Z.S. Li, Z.G. Zou, Langmuir 26 (2010) 3894–3900.
- [21] G.H. Dong, K. Zhao, L.Z. Zhang, Chem. Commun. 48 (2012) 6178–6180.
- [22] J.H. Li, B.A. Shen, Z.H. Hong, B.Z. Lin, B.F. Gao, Y.L. Chen, Chem. Commun. 48 (2012) 12017–12019.
- [23] J.S. Zhang, G.G. Zhang, X.F. Chen, S. Lin, L. Mohlmann, G. Dolega, G. Lipner, M. Antonietti, S. Blechert, X.C. Wang, Angew. Chem. Int. Ed. 51 (2012) 3183–3187.
- [24] M. Shalom, S. Inal, C. Fetteckhauer, D. Neher, M. Antonietti, J. Am. Chem. Soc. 135 (2013) 7118–7121.
- [25] K. Schwinghammer, B. Tuffy, M.B. Mesch, E. Wirnhier, C. Martineau, F. Taulelle, W. Schnick, J. Senker, B.V. Lotsch, Angew. Chem. Int. Ed. 52 (2013) 2435–2439.
- [26] Z. Lin, X. Wang, Angew. Chem. Int. Ed. 52 (2013) 1735–1738.
- [27] M. Zhang, X. Wang, Energy Environ. Sci. 7 (2014) 1902–1906.
- [28] J. Zhang, X. Chen, K. Takanabe, K. Maeda, K. Domen, J.D. Epping, X. Fu, M. Antonietti, X. Wang, Angew. Chem. Int. Ed. 49 (2010) 441–444.
- [29] J. Zhang, M. Zhang, S. Lin, X. Fu, X. Wang, J. Catal. 310 (2014) 24–30.
- [30] Y. Chen, J. Zhang, M. Zhang, X. Wang, Chem. Sci. 4 (2013) 3244–3248.
- [31] A.D. Becke, J. Chem. Phys. 98 (1993) 5648–5652.
- [32] M. Tabbal, T. Christidis, S. Isber, P. Mèrel, M.A. El Khakani, M. Chaker, A. Amassian, L. Martinu, J. Appl. Phys. 98 (2005) 44310.
- [33] Y. Cui, Z. Ding, P. Liu, M. Antonietti, X. Fu, X. Wang, Phys. Chem. Chem. Phys. 14 (2012) 1455–1462.
- [34] Z. Chen, W. Wang, Z. Zhang, X. Fang, J. Phys. Chem. C 117 (2013) 19346–19352.